Structural, vibrational, and quasiparticle properties of the Peierls semiconductor $BaBiO_3$: A hybrid functional and self-consistent GW+vertex-corrections study

C. Franchini,[1] A. Sanna,[2] M. Marsman,[1] and G. Kresse[1]

[1]*Faculty of Physics, Universität Wien and Center for Computational Materials Science, Sensengasse 8, A-1090 Wien, Austria*

[2]*Department of Physics, Sardinian Laboratory for Computational Materials Science (SLACS), INFM-CNR, University of Cagliari, Cittadella Universitaria, Monserrato, I-09024 Cagliari, Italy*

(Received 18 November 2009; published 23 February 2010)

$BaBiO_3$ is characterized by a charge disproportionation with half of the Bi atoms possessing a valence 3+ and half a valence 5+. Because of self-interaction errors, local- and semilocal-density functionals fail to describe the charge disproportionation quantitatively, yielding a too small structural distortion and no band gap. Using hybrid functionals, we obtain a satisfactory description of the structural, electronic, optical, and vibrational properties of $BaBiO_3$. The results obtained using GW (Green's function G and screened Coulomb potential W) based schemes on top of hybrid functionals, including fully self-consistent GW calculations with vertex corrections in the dielectric screening, qualitatively confirm the Heyd-Scuseria-Ernzerhof picture but a systematic overestimation of the band gap by about 0.4 eV is observed.

DOI: 10.1103/PhysRevB.81.085213 PACS number(s): 71.45.Lr, 71.20.Nr, 71.35.−y, 78.20.−e

I. INTRODUCTION

The Peierls semiconductor $BaBiO_3$, parent compound of the high-T_c superconductor $Ba_{1-x}K_xBiO_3$, has long been of theoretical and experimental interest due to its distinct negative-U nature. This behavior can be understood through the concept of "forbidden valence" suggesting that in $BaBiO_3$ bismuth atoms appear in two different valences (5+ and 3+) but *skip* the forbidden formal valence in between (4+). The "valence-skipper" bismuth atoms hence disproportionate, i.e., every second Bi atom donates all 5 valence electrons to oxygen whereas the other Bi atom retains two 6*s* electrons and only donates the three 6*p* electrons to the oxygen atoms. Such a behavior is usually explained by the concept of a negative U which invalidates the usual positive Coulomb repulsion between two electrons.[1] The charge disproportionation goes in hand with significant structural changes from the ideal cubic perovskite crystal toward a distorted monoclinic structure characterized by a short-ranged charge-density wave (CDW) state formed by alternating breathing-in and breathing-out distortions of oxygen octahedra around inequivalent Bi^{5+} (Bi1) and Bi^{3+} (Bi2) ions (Fig. 1). As a consequence of this charge ordering, the formally expected metallic state for the cubic perovskite $BaBi^{4+}O_3$ is replaced by an insulating regime characterized by a large direct CDW optical response $E_d \approx 2.0$ eV (Ref. 2) and an indirect optical transition E_i. Although $BaBiO_3$ has been the subject of numerous optical investigations, dissenting opinions were reported on the value of the indirect gap E_i, for which conflicting measurements are reported in literature, ranging from 0.2 (Ref. 3) to 1.1 eV.[4]

Despite the apparent absence of strong electron localization usually associated with *d* and *f* electrons, standard semilocal-density functionals exhibit severe problems in describing the basic properties of this material, yielding much too small or even negative band gaps,[4,5] thus preventing a detailed description of the electronic properties. In a recent paper, we have explained the polaron-mediated insulator-to-metal transition experimentally observed in K-doped $BaBiO_3$ by means of hybrid density-functional theory. We have shown that semilocal functionals are incapable (i) to disclose the underlying physics of this type of electronic transition and, more generally, (ii) to account for "long-range" Peierls-type distortions in doped $BaBiO_3$.[6] The objective of the present study is to apply the screened exchange hybrid density-functional theory (DFT) Heyd-Scuseria-Ernzerhof (HSE) functional[7] to the ground-state structural, electronic, and vibrational properties of $BaBiO_3$, and to investigate to which extent many-body effects may alter the ground-state and quasiparticle (QP) properties of $BaBiO_3$. We address the latter issue by adopting the GW approach. These calculations essentially confirm the picture emerging from the hybrid functional. Details of our computational approach are described in the methodological section whereas the results are presented and discussed in Sec. III.

II. METHODOLOGY

We have used the projector-augmented wave (PAW) method[8,9]-based Vienna *ab initio* simulation package (VASP)

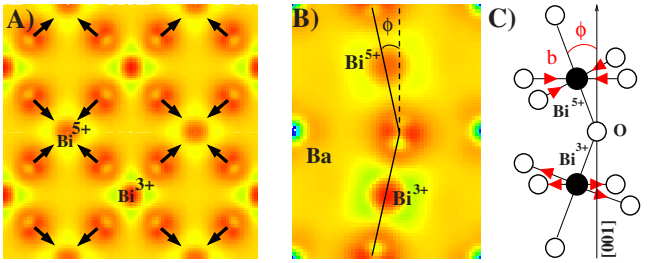

FIG. 1. (Color online) Self-consistent-GW charge-density plots showing (a) the breathing distortion in the (100) plane and (b) the tilting instability projected in the (001) plane. Bi^{5+} (Bi1) and Bi^{3+} (Bi2) indicate the two inequivalent bismuth ions whereas the arrows indicate the breathing displacement of the oxygen atoms. (c) Schematic view of the $BaBiO_3$ unit cell showing the BiO_6 tilted octahedra. Color coding: darker (red) areas indicates a high value of the charge density.

(Ref. 10) employing the generalized gradient approximation scheme of Perdew *et al.*[11] (PBE), the HSE hybrid functional,[12] and the GW formalism.[13,14] The HSE functional is constructed by mixing 25% of the exact Hartree-Fock exchange with 75% of the Perdew-Burke-Ernzerhof (PBE) exchange functional.[7] The resulting expression for the exchange (x) and correlation (c) energy is

$$E_{xc}^{\mathrm{HSE03}} = E_x^{\mathrm{PBE}} - \frac{1}{4}E_x^{\mathrm{PBE,sr},\mu} + \frac{1}{4}E_x^{\mathrm{HF,sr},\mu} + E_c^{\mathrm{PBE}}, \qquad (1)$$

in which the parameter μ controls the decomposition of the Coulomb kernel into short-range (sr) and long-range contributions to the exchange. $E_x^{\mathrm{HF,sr},\mu}$ is the exact exchange screened at very long range and $E_x^{\mathrm{PBE,sr},\mu}$ is the corresponding short-range exchange functional constructed using the PBE exchange hole. According to the HSE06 recipe, we set $\mu = 0.2$ Å^{-1}.[15] This implies that nonlocal exchange is rather long ranged extending over several nearest-neighbor shells. The HSE approach has been used to calculate the starting orbitals for different GW-based schemes of increasing complexity and precision in the evaluation of the self-energy $\Sigma = i\mathrm{GW}$. The screened Coulomb kernel $\mathrm{W} = \epsilon^{-1}v$ which enters in the previous expression requires the computation of the frequency-dependent dielectric matrix $\epsilon^{-1} = 1 + v\chi$, where the polarizability χ is given by the Dyson equation

$$\chi = [1 - \chi_0(v + f_{xc})]^{-1}\chi_0. \qquad (2)$$

Here, χ_0 indicates the independent-particle polarizability whereas f_{xc} represents the effective nonlocal exchange-correlation kernel which describes the many-body interaction between electrons and holes (vertex corrections). We have adopted three different GW strategies: (i) the widely used single-shot (i.e., nonself-consistent) $\mathrm{G_0W_0}$ approximation, where $\mathrm{G_0}$ and $\mathrm{W_0}$ are calculated using HSE eigenvalues and eigenfunctions within the so-called random-phase approximation (RPA) (i.e., excluding any vertex corrections, $f_{xc}=0$).[16] The VASP implementation is detailed in Refs. 13 and 14. Using HSE orbitals, this approach usually slightly overestimates the band gap but is very efficient.[17]

(ii) A partially self-consistent procedure consisting of an update of the eigenvalues in the Green's function G combined with HSE screening properties $\mathrm{W_0}(\mathrm{GW_0})$. Within this scheme, we have included electrostatic electron-hole interactions in the computation of W using time-dependent HSE (TD-HSE) through an effective nonlocal frequency-independent kernel f_{xc}. This specific GW scheme, usually denoted as $\mathrm{GW_0^{TCTC}}$ (test charge/test charge $\mathrm{GW_0}$), is believed to remedy most of the problems of single-shot $\mathrm{G_0W_0}$ and is considered to be a convenient (less time consuming) and trustable (experimental precision) alternative to fully self-consistent GW. The approach was found to yield excellent QP band gaps in simple *sp*-bonded semiconductors, if and only if the electrostatic interactions between electrons and holes were taken into account.[18] The electrostatic electron-hole interaction is included using an effective many-electron exchange-correlation kernel constructed using the HSE functional (Nanoquanta kernel determined to mimic TD-HSE, for details we refer to Refs. 19–22).

(iii) Finally, we employ the self-consistent quasiparticle GW ($\mathrm{scQPGW^{TCTC}}$), following the original ideas of Faleev, Schilgaarde, and Kotani,[23,24] with the inclusion of vertex corrections adopting the formalism of Reining *et al.*[19–22] [Nanoquanta kernel constructed to mimic the Bethe-Salpeter equation (BSE)]. This approach is rather time consuming but entirely free of any dependence on the starting orbitals. For *sp*-bonded materials, it yields band gaps within a few percent of experiment, if the electrostatic electron-hole interaction is included using a many-electron exchange-correlation kernel f_{xc}.[25]

The simulated unit cell, containing ten atoms, has been modeled using a $4\times4\times4$ *k*-point grid and an energy cutoff of 400 eV, reduced to 300 eV within GW calculations. To calculate the frequency-dependent dielectric matrix, the inclusion of 400 empty bands was sufficient to obtain well-converged screening properties and QP eigenvalues, substantially larger than the corresponding number of empty bands included in the PBE and HSE runs (15) whereas the calculation of the local fields effects has been performed for 35 bands around the Fermi energy. For the GW calculations, a suitably optimized PAW pseudopotential data set was employed which allow for a more accurate treatment of the conduction bands, as discussed in more detail in Refs. 14 and 24. We have adopted core radii of 3.740 a.u, 3.090 a.u., and 1.85 a.u, for Ba, Bi, and O, respectively, and included the Bi 5*d* and Ba 5*s* and 5*p* states in the valence shell.

III. RESULTS AND DISCUSSION

A. Structure

The low-temperature phase of $\mathrm{BaBiO_3}$ is monoclinic and derives from the primitive cubic perovskite high-temperature cell by simultaneous breathing (b) and tilting (ϕ) distortions of the octahedra[26] (Fig. 1). Unlike previous studies, we have performed a full structural relaxation by allowing for both b and ϕ distortions as well as for volume (V) and shape (β, the monoclinic angle) optimization. The resulting minimized geometries listed in Table I reveal that the structural properties are sensitive to the applied functional and are generally better reproduced within HSE. In particular, the PBE functional seriously overestimates the volume ($\approx$4%), which is in fact well described using HSE. Also, the breathing displacement, which is responsible for the opening of the CDW gap,[4] is better described using the hybrid functional. The minimum HSE Bi-O bond-length splitting $b=0.09$ Å matches exactly the experimental value. The volume and, to a lesser extent, the breathing displacement does not improve by using a revised version of the PBE functional designed to yield improved equilibrium volumes, the so-called PBEsol functional[27] (see Table I).

B. Electronic properties

The approximations made in the exchange-correlation term, have an even more drastic impact on the predicted electronic and dielectric properties. In line with past findings, PBE predicts a zero-gap system ($E_i^{\mathrm{PBE}}=0.0$ eV) with a much too small direct band gap $E_d(E_d^{\mathrm{PBE}}=1.22$ eV). Although the

TABLE I. Collection of calculated quantities along with the available experimental data. The abbreviations V (volume), b (breathing distortion), ϕ (tilting distortion), β (monoclinic angle), E_d (direct gap), E_i (indirect gap), and ϵ_∞ (macroscopic dielectric constant) are described in the text and, partially, in Fig. 1(c).

	PBE (This work)	PBEsol (This work)	HSE (This work)	G_0W_0 (This work)	GW (This work)	GW_0^{TCTC} (This work)	$scQPGW^{TCTC}$ (This work)	LMTO-LDA (Ref. 4)	PAW-LDA (Ref. 5)	Expt.
V (Å^3)	85.76	85.94	82.10					80.41	81.04	82.21[a]
b (Å)	0.07	0.075	0.09					0.11	0.04	0.085[a]
ϕ (deg)	12.1	12.2	11.9					9.6		11.2[a]
β (deg)	90.16	90.14	90.24							90.17[a]
E_d (eV)	1.22	1.32	2.07	2.62	3.00	2.39	2.45	1.1		2.0[b]
E_i (eV)	0.0	0.0	0.84	1.32	1.63	1.15	1.28	0.1	0.0	0.2[c], 0.5[d], 0.8[e], 1.1[f]
ϵ_∞	12.2		6.0		4.5	7.0	7.2			5[g], 7[h]

[a]Reference 26.
[b]Reference 2.
[c]Reference 3.
[d]Reference 28.
[e]Reference 29.
[f]Reference 4.
[g]Reference 30.
[h]Reference 31.

origin of this failure has often been related to the deficient description of the structural instabilities at the PBE level, we found that the values E_i^{PBE} and E_d^{PBE} computed adopting the HSE and experimental geometries are only 0.05 meV larger than those calculated at the PBE structural minimum, and therefore still in conflict with the experimental measurements.

In order to capture the insulating character of $BaBiO_3$, we have adopted the HSE functional and the GW method at the three levels described in the methodological section. The computed band structure is shown in Fig. 2, where we plot the most relevant bands near the Fermi level (E_F=0) for PBE, HSE, G_0W_0, GW_0^{TCTC}, and $scQPGW^{TCTC}$. We observe

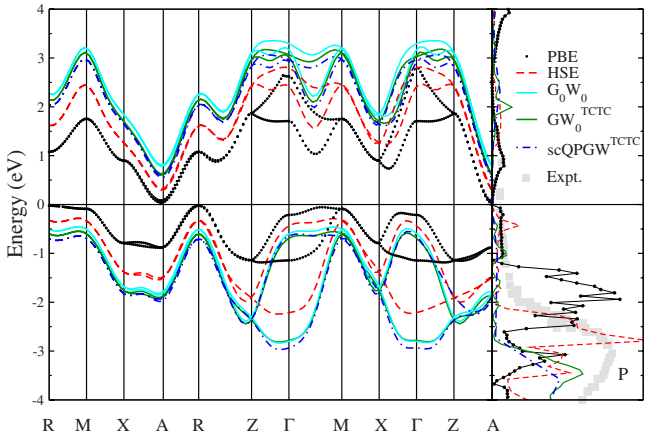

FIG. 2. (Color online) Calculated (left) band structure of monoclinic $BaBiO_3$ within PBE, HSE G_0W_0, GW_0^{TCTC}, and $scQPGW^{TCTC}$ and (right) corresponding total density of states. The reciprocal space direct coordinates of the selected high-symmetry k points for the monoclinically distorted supercell reads: $\Gamma(0,0,0)$, $R(0,\frac{1}{2},\frac{1}{2})$, $M(\frac{1}{2},\frac{1}{2},0)$, $X(\frac{1}{2},0,0)$, and $A(\frac{1}{2},0,\frac{1}{2})$. E_i is opened between the A and R points of our modeled supercell, which correspond to the W and L points of the ideal undistorted fcc cell (Ref. 5). P refer to the measured main photoemission peak of the valence i band (Ref. 32).

that the pragmatic inclusion of 25% nonlocal Hartree-Fock exchange within the HSE approach shifts apart the bands near E_F and increases both E_i (0.84 eV) and E_d (2.07 eV). These values are in good agreement with the available measurements.

The G_0W_0 approximation evaluated using HSE orbitals further increases the band gap between the occupied and empty states resulting in significantly larger quasiparticle gaps than HSE (see Table I). The update of the eigenvalues in G and, in particular, the inclusion of e-h (electron-hole) interactions (GW_0^{TCTC}) leads to a slight reduction in the quasiparticle band gaps (≈4%). We note that the former approach (G_0W_0) is known to overestimate the band gaps for s-p-bonded semiconductors and insulators using HSE orbitals by typically 10% (Refs. 17 and 18) whereas the latter approach (GW_0^{TCTC}) yields very good values almost on par with fully self-consistent $scQPGW^{TCTC}$ calculations.[18,25] Indeed, in this specific material, the $scQPGW^{TCTC}$ band structure is very close to the GW_0^{TCTC} band structure, although the indirect band gap increases slightly from 1.15 to 1.28 eV. Full self-consistent GW without vertex corrections (GW in Table I) leads to significantly larger band gaps (E_d =3.00 eV and E_i=1.63 eV) than $scQPGW^{TCTC}$, due to the neglection of any electron-hole attractive interaction. Unfortunately, the experimental uncertainty in E_i does not permit to ascertain which method yields the most accurate results but the GW values are generally somewhat larger than the maximum values determined experimentally. Since the direct gap E_d has been measured using optical techniques, it is possibly impaired by excitonic effects (see below) but overall it seems that GW does yield a slightly too large band gaps for $BaBiO_3$. However, compared to photoemission data,[32] the calculated total density of states (shown on the right side of Fig. 2) show that GW_0^{TCTC} and $scQPGW^{TCTC}$ yield a main valence-band peak (≈−3.4 eV) in much better agreement with experiment (−3.2 eV) than PBE (−1.9 eV) and HSE (−2.8 eV). Once more, we underline the need of more detailed experimental data to unequivocally probe the predictive power of GW-type and HSE calculations. It should also

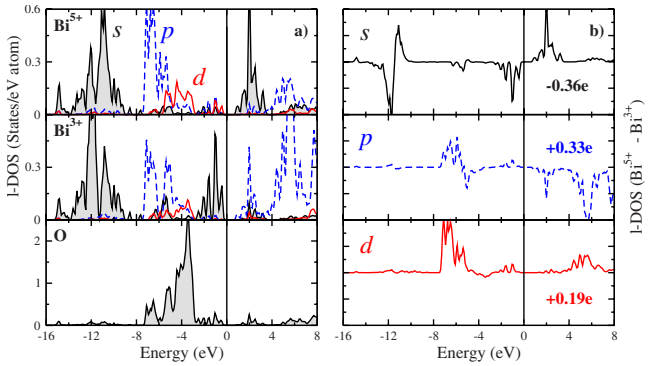

FIG. 3. (Color online) Calculated scQPGW^{TCTC} (a) partial DOS decomposed over Bi1, Bi2 and O (apical and planar oxygen yield identical DOS) and (b) DOS difference between Bi1 and Bi2 decomposed into l quantum numbers.

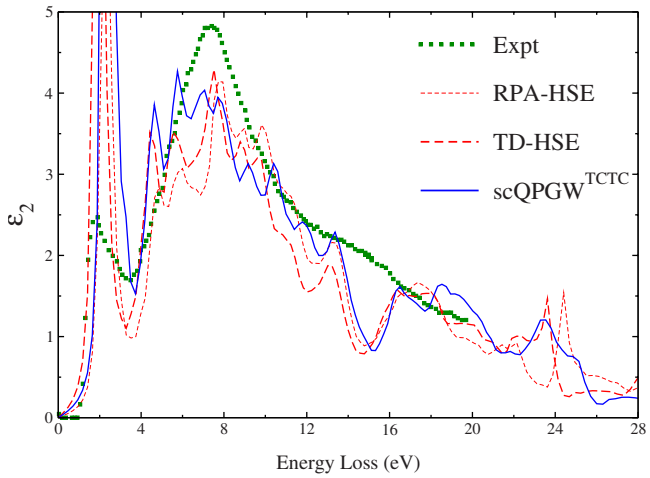

FIG. 4. (Color online) The imaginary parts of the dielectric function (ϵ_2) are shown for RPA-HSE, TD-HSE, and scQPGW^{TCTC} along with the experimental curve from Ref. 38.

be stressed that GW-like approaches, though employed for more than 20 years, have been applied so far mainly to prototypical semiconductors and insulators (GaS, ZnO, Cu_2O, etc.,…) but, their performance on more complex systems such as $BaBiO_3$, has been assessed for a limited number of cases only [LaMO_3(M=Ti Cu),[33] V_2O_3,[34] and VO_2 (Refs. 35 and 36)]. A comparison with accurate experimental measurements is therefore essential.

Let us proceed to shed light on the nature of the CDW gap E_i. It is accepted that E_i is formed by the splitting of the conduction Bi(s)-O(p) antibonding orbitals into two subbands but the electronic charge redistribution has not been discussed in details. Figure 3(a) reports the scQPGW^{TCTC} l-projected density of states (DOS) on Bi and O sites which should be interpreted in conjunction with the band-projected charge (Table II). The formation of the CDW lowers the symmetry of the crystal thus inducing a global rearrangement of the charge around the two inequivalent Bi sites (see Fig. 1). We find that E_i is opened between occupied Bi2(s) states (valence-band maximum) and empty Bi1(s)-Bi2(p_xp_y) orbitals (conduction-band minimum). This orbital-ordered insulating state is indeed more complex than the generally accepted picture invoking a simple Bi(s)-O(p) gap and arises from the elaborate nature of the charge disproportionation, resulting in the electronic states shown in Fig. 3(b).

TABLE II. scQPGW^{TCTC}, HSE and PBE band-projected charge (in partial number of electrons e^-) on Bi1 and Bi2. Charges have been determined inside the PAW spheres.

	s	p	d
		scQPGW^{TCTC}	
Bi1	1.280	1.199	10.254
Bi2	1.642	0.871	10.065
Bi1-Bi2	−0.36	+0.33	+0.19
		HSE	
Bi1	1.318	1.176	10.252
Bi2	1.694	0.830	10.063
Bi1-Bi2	−0.38	+0.35	+0.19
		PBE	
Bi1	1.371	1.085	10.181
Bi2	1.623	0.863	10.056
Bi1-Bi2	−0.25	+0.22	+0.13

Previous calculations[4,37] argued that the static valence charge difference δ between Bi1 and Bi2 is not significant. The calculated δ is indeed rather small ($\delta_{PBE}=0.10e^-$, $\delta_{HSE}=0.16e^-$, $\delta_{scQPGW^{TCTC}}\approx 0.16e^-$) but it is the result of a substantial transfer involving orbitals with different angular moments. HSE and GW provide essentially the same picture whereas PBE underestimates significantly the l-decomposed charge transfer by about 30% (see Table II). In more detail, the flow of charge induced by the charge disproportionation between Bi1 and Bi2 involves a s-like charge transfer from Bi1 to Bi2 ($0.36e^-$) which is compensated by a backtransfer of p ($0.33e^-$) and d ($0.16e^-$) charge mostly localized in the energy range from −8 to −4 eV. This backtransfer can be understood by realizing that the O atoms are much closer to Bi1. As a result, the tails of the O(p) orbitals overlap with the Bi1 spheres and are picked up as states with higher angular momentum specifically p- and d-like character.

C. Optical and dielectric properties

In addition to the formation of a band gap, the CDW also causes a strong optical resonance at ≈2 eV. In Fig. 4, we compare the experimental imaginary part of the dielectric function ϵ_2 (Ref. 38) with the theoretical spectrum computed within different approximations: (i) the RPA using HSE orbitals, (ii) TD-HSE (as described in Ref. 18), and (iii) TD-scQPGW^{TCTC}. The first approach (i) neglects any electrostatic interactions between electrons and holes. The second approach (ii) is similar to TD Hartree-Fock but the electrostatic interaction between electrons and holes is only 1/4—more precisely it is described by the sr-exchange kernel in HSE—whereas in the final approach (iii) the interaction between electrons and holes is described fully *ab initio* using

the W determined in the scQPGW calculations. For (i) and (ii), HSE orbitals and one-electron energies are used whereas (iii) is based on the scQPGW one-electron energies and orbitals, and the results of (iii) are usually equivalent to Bethe-Salpeter calculations without the Tamm-Dankof approximation.[18,20]

Considering the complexity of the system, the agreement is remarkably good with regard to the position and the width of the two dominant peaks, namely, the CDW peak at 2 eV and the excitation at 8.0 eV, which can be described as the transition from the main peak of the valence band (−3.4 eV) to the broad group of states starting at about 4 eV above E_F. The overestimation of the intensity of the CDW peak is most likely related to a too coarse k-point sampling. Unfortunately, in this fairly complex system, calculations with a denser k-point grid are very time consuming, and we do not expect that they will change the results qualitatively. The first important observation is that there is a difference between the RPA-HSE and TD-HSE calculations. Excitonic effects (e-h interaction) shift the CDW peak down by approximately 0.3–0.4 eV. The scQPGW calculations, which also include excitonic effects, predict a blueshifted CDW excitation ≈0.2–0.4 eV above the experimental peak. Unfortunately, this confirms that the scQPGW overestimates the direct band gap somewhat, as was already hinted at in the section on the electronic properties.

Finally, we calculated the ion-clamped (high frequency) macroscopic dielectric constant ϵ_∞ (Table I). The HSE ϵ_∞ was computed adopting the perturbation expansion after discretization (PEAD) method.[39] Within the PEAD method, we applied a finite field in the supercell and extracted the static dielectric constant from the resultant macroscopic field. This approach includes local-field effects (electron-hole interactions). The so obtained macroscopic dielectric constant ($\epsilon_\infty^{\mathrm{HSE}}=6$) is in good agreement with the experimental estimations (5 and 7, see Table I) extracted through a fit of the reflectivity spectra. The GW_0 and scQPGW values, 7.0 and 7.2, respectively, though still in good agreement with experiment are about 15% larger than the HSE values. As expected from the serious underestimation of the gap, TD-PBE fails dramatically in predicting $\epsilon_\infty(\epsilon_\infty^{\mathrm{PBE}}=12.2)$.

D. Phonons and infrared reflectivity

We conclude our analysis by exploring the effect of nonlocal exchange on the zone-centered phonon frequencies and on the oscillator strengths of the infrared (IR) reflectivity active modes. Since within the GW method, the calculation of phonon frequencies is presently out of reach, we focus on PBE and HSE only. The evaluation of the Born effective charge (BEC) $Z^*_{i,\alpha\beta}$, required for the calculation of the IR spectra, were performed adopting the PEAD (HSE) and linear-response (PBE) methods. Excluding the three acoustic modes (which are zero at Γ), the monoclinic phase (containing ten atoms per unit cell) possesses 27 optical modes with the symmetry,

$$7A_g + 5B_g + 6A_u + 9B_u.$$

The *gerade* modes are Raman active and the *ungerade* modes are infrared active. In Fig. 5, we compare our calculated HSE IR spectra with the experimental reflectivity data.[40] The results are remarkable; the inclusion of nonlocal exchange is essential to account for a correct prediction of the phonon modes with large oscillator strength. The three highest modes at 157, 256, and 463 cm^{-1} reproduce very well the corresponding experimental values whereas the lowest mode at 119 cm^{-1} is shifted upward with respect to the measured one by ≈20 cm^{-1}. In addition, we find that the highest-frequency phonon (Raman active) corresponding to the BiO_6 breathing mode responsible for the CDW instability, experiences a huge shift from PBE (453 cm^{-1}) to HSE (562 cm^{-1}). The HSE value coincides with the value provided by Raman-scattering analysis,[41] 570 cm^{-1}. The problems of PBE can be attributed primarily to volume effects. Due to the large PBE volume, the PBE phonon vibrations are located at lower frequencies. In addition to this, we note that the PBE inadequate description of the oxygen breathing distortions is also reflected in the phonon spectra. The frequency downshift is larger (45–60 cm^{-1}) for the oxygen-based modes lying at higher frequency than for the lower modes (20–30 cm^{-1}) emerging from the softer Bi and Ba vibrations which are actually very well described at the PBE level. A similar behavior has been observed in ZnO.[42]

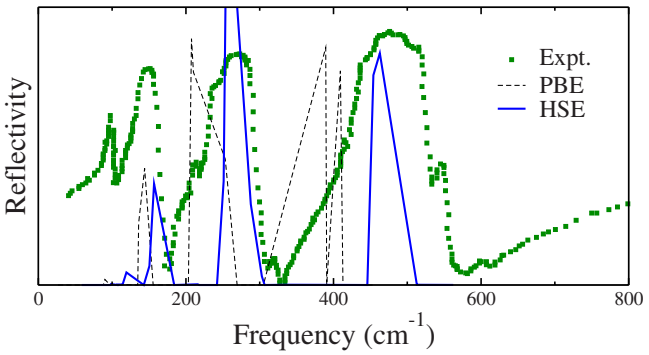

FIG. 5. (Color online) Comparison between calculated and measured (Ref. 40) infrared reflectivity.

Finally, we list in Table III the computed BEC $Z^*_{i,\alpha\beta}$. We find that the BEC tensor is diagonal and reduces to a scalar matrix for Ba and Bi (i.e., $Z^*_{\mathrm{Ba/Bi},11}=Z^*_{\mathrm{Ba/Bi},22}=Z^*_{\mathrm{Ba/Bi},33}$) and to two components $Z^*_\parallel$ and $Z^*_\perp$ for O with respect to the Bi-O bond. In agreement with precedent estimations of Thonhauser and Rabe,[5] we observe a significant BEC disproportionation between Bi1 and B2 ($Z^*_{\mathrm{Bi2}}-Z^*_{\mathrm{Bi1}}$), substantially larger than the corresponding static charge transfer δ discussed above (see Table II). The incorporation of nonlocal exchange effects through HSE reduces the dynamical charge disproportionation from $1.66|e^-|$ (PBE) to $0.97|e^-|$ (HSE) and leaves the Ba and O BEC's unchanged. The average BEC of oxygen $-3.13|e^-|$ equals the experimentally derived value of $-3.2|e^-|$.[31]

IV. SUMMARY

In summary, by means of beyond-DFT methods we have computed ground-state and excited-state properties of $BaBiO_3$. On the basis of hybrid functionals and fully *ab ini-*

TABLE III. Calculated HSE and PBE Born effective charges $Z^*_{i,\alpha\beta}$ (with i atom index) in unit of $|e^-|$. $Z^*_\parallel$ and $Z^*_\perp$ refers to the components parallel and perpendicular to the Bi-O bond. The LDA values are taken from Ref. 5.

	Bi1	Bi2	Ba	O
			HSE	
$Z^*_{i,\alpha\alpha}$	5.01	5.98	2.71	
$Z^*_\parallel$				−4.39
$Z^*_\perp$				−1.88
			PBE	
$Z^*_{i,\alpha\alpha}$	4.65	6.31	2.71	
$Z^*_\parallel$				−4.36
$Z^*_\perp$				−1.89
			LDA (Ref. 5)	
$Z^*_{i,\alpha\alpha}$	4.78	6.22	2.75	
$Z^*_\parallel$				−4.55
$Z^*_\perp$				−1.85

tio GW methods, we have shown that the inclusion of nonlocal exchange effects is essential to reproduce and understand the complex physical properties of $BaBiO_3$. Our calculated structural distortions (oxygen instabilities and cubic-to-monoclinic transition), optical excitations (direct/indirect band gap and optical spectrum), dielectric (dielectric constant) and vibrational properties (phonon frequencies, infrared reflectivity, and Born effective charges) reproduce well the available experimental findings. Overall, our study suggests that the GW approaches tend to overestimate the band gap, which seems to be better predicted within the screened hybrid HSE functional. Although the inclusion of an effective nonlocal exchange-correlation kernel f_{xc} at TD-HSE (GW_0^{TCTC}) and BSE-GW ($scQPGW^{TCTC}$) level improves the single-shot G_0W_0 description, the resulting band gap is still $\approx 15\%(E_d)$ and 40% (E_i) larger than the corresponding *bare* HSE value. The source of this error as far as it cannot be attributed to uncertainties in the experimental results likely resides in the neglect of many-body vertex corrections in the self-energy Σ, which are entirely neglected in this work or any other GW implementation. Though $scQPGW^{TCTC}$ has proven to be excellent for the prediction of the band gaps of typical semiconductor, insulator, and noble gas solids it was never applied to more complex oxides such as $BaBiO_3$. Given the lack of accurate experimental information on the electronic properties of $BaBiO_3$ (especially for the indirect gap E_i), the assessment of these GW techniques to less critical oxides for which well-established experimental data exists is highly required.

Concluding our research on $BaBiO_3$ clarifies the serious drawbacks of standard DFT and provide a key to understand and design similar charge-ordered materials. We hope that our study can boost for future experiments as well as for thorough theoretical and computational efforts aiming to straighten the issues still under debate. Furthermore, we have shown that the hybrid functional HSE yields a description which is at least on par with sophisticated many-body techniques.

ACKNOWLEDGMENT

This work was supported by the European Community FP7 project ATHENA.

[1] W. A. Harrison, Phys. Rev. B **74**, 245128 (2006).
[2] Uchida, K. Kitazawa, and S. Tanaka, Phase Transitions **8**, 95 (1987).
[3] A. W. Sleight, J. L. Gillson, and P. E. Bierstedt, Solid State Commun. **17**, 27 (1975).
[4] K. Kunc, R. Zeyher, A. I. Liechtenstein, M. Methfessel, and O. K. Andersen, Solid State Commun. **80**, 325 (1991).
[5] T. Thonhauser and K. M. Rabe, Phys. Rev. B **73**, 212106 (2006).
[6] C. Franchini, G. Kresse, and R. Podloucky, Phys. Rev. Lett. **102**, 256402 (2009).
[7] J. Heyd, G. E. Scuseria, and M. Ernzerhof, J. Chem. Phys. **118**, 8207 (2003).
[8] P. E. Blöchl, Phys. Rev. B **50**, 17953 (1994).
[9] G. Kresse and D. Joubert, Phys. Rev. B **59**, 1758 (1999).
[10] G. Kresse and J. Furthmüller, Comput. Mater. Sci. **6**, 15 (1996).
[11] J. P. Perdew, K. Burke, and M. Ernzerhof, Phys. Rev. Lett. **77**, 3865 (1996).
[12] J. Paier, R. Hirschl, M. Marsman, and G. Kresse, J. Chem. Phys. **122**, 234102 (2005).
[13] M. Shishkin and G. Kresse, Phys. Rev. B **74**, 035101 (2006).
[14] M. Shishkin and G. Kresse, Phys. Rev. B **75**, 235102 (2007).
[15] A. V. Krukau, O. A. Vydrov, A. F. Izmaylov, and G. E. Scuseria, J. Chem. Phys. **125**, 224106 (2006).
[16] M. S. Hybertsen and S. G. Louie, Phys. Rev. B **34**, 5390 (1986).
[17] F. Fuchs, J. Furthmüller, F. Bechstedt, M. Shishkin, and G. Kresse, Phys. Rev. B **76**, 115109 (2007).
[18] J. Paier, M. Marsman, G. Kresse, Phys. Rev. B **78**, 121201(R) (2008).
[19] L. Reining, V. Olevano, A. Rubio, and G. Onida, Phys. Rev. Lett. **88**, 066404 (2002).
[20] F. Sottile, V. Olevano, and L. Reining, Phys. Rev. Lett. **91**, 056402 (2003).
[21] G. Adragna, R. Del Sole, and A. Marini, Phys. Rev. B **68**, 165108 (2003).
[22] F. Bruneval, F. Sottile, V. Olevano, R. Del Sole, and L. Reining, Phys. Rev. Lett. **94**, 186402 (2005).
[23] M. van Schilfgaarde, T. Kotani, and S. Faleev, Phys. Rev. Lett. **96**, 226402 (2006).
[24] S. V. Faleev, M. van Schilfgaarde, and T. Kotani, Phys. Rev. Lett. **93**, 126406 (2004).
[25] M. Shishkin, M. Marsman, and G. Kresse, Phys. Rev. Lett. **99**, 246403 (2007).
[26] D. E. Cox and A. W. Sleight, Solid State Commun. **19**, 969 (1976); Acta Crystallogr., Sect. B: Struct. Crystallogr. Cryst.

Chem. **35**, 1 (1979).
[27] J. P. Perdew, A. Ruzsinszky, G. I. Csonka, O. A. Vydrov, G. E. Scuseria, L. A. Constantin, X. Zhou, and K. Burke, Phys. Rev. Lett. **100**, 136406 (2008).
[28] H. Takagi, S. Uchida, S. Tajima, K. Kitazawa, and S. Tanaka, *Proceedings of the International Conference on the Physics of Semiconductors*, Stockholm, edited by O. Engstrom (World Scientific, Singapore, 1986), p. 1851.
[29] K. H. Kim, C. U. Jung, T. W. Noh, and S. C. Kim, Phys. Rev. B **55**, 15393 (1997).
[30] S. Tajima, S. Uchida, A. Masaki, H. Takagi, K. Kitazawa, S. Tanaka, and A. Katsui, Phys. Rev. B **32**, 6302 (1985).
[31] T. Nishio and H. Uwe, J. Phys. Soc. Jpn. **72**, 1274 (2003).
[32] Z.-X. Shen, P. A. P. Lindberg, B. O. Wells, D. S. Dessau, A. Borg, I. Lindau, W. E. Spicer, W. P. Ellis, G. H. Kwei, K. C. Ott, J.-S. Kang, and J. W. Allen, Phys. Rev. B **40**, 6912 (1989).
[33] Y. Nohara, S. Yamamoto, and T. Fujiwara, Phys. Rev. B **79**, 195110 (2009).
[34] E. Papalazarou, Matteo Gatti, M. Marsi, V. Brouet, F. Iori, Lucia Reining, E. Annese, I. Vobornik, F. Offi, A. Fondacaro, S. Huotari, P. Lacovig, O. Tjernberg, N. B. Brookes, M. Sacchi, P. Metcalf, and G. Panaccione, Phys. Rev. B **80**, 155115 (2009).
[35] M. Gatti, F. Bruneva, V. Olevano, and L. Reining, Phys. Rev. Lett. **99**, 266402 (2007).
[36] R. Sakuma, T. Miyake1, and F. Aryasetiawan, Phys. Rev. B **78**, 075106 (2008).
[37] L. F. Mattheiss and D. R. Hamann, Phys. Rev. B **28**, 4227 (1983).
[38] Y.-Y. Wang, G. F. Feng, T. E. Sutto, and Z. Shao, Phys. Rev. B **44**, 7098 (1991).
[39] R. W. Nunes and X. Gonze, Phys. Rev. B **63**, 155107 (2001).
[40] R. P. S. M. Lobo and F. Gervais, Phys. Rev. B **52**, 13294 (1995).
[41] S. Sugai, S. Uchida, K. Kitazawa, S. Tanaka, and A. Katsui, Phys. Rev. Lett. **55**, 426 (1985).
[42] J. Wróbel, K. J. Kurzydlowski, K. Hummer, G. Kresse, and J. Piechota, Phys. Rev. B **80**, 155124 (2009).